

## Covalent shaping of polyoxometalate molecular films onto ITO electrodes for charge trapping induced resistive switching

Raphaël Salles, Wei Church Poh, Maxime Laurans, Florence Volatron, Antoine Miche, Sandra Alves, Christian Carino, Ludovic Tortech, Guillaume Izet, Pooi See Lee,\* Anna Proust\*

### Supporting Information

#### Contents

##### Synthesis and characterizations of $(TBA)_4[PW_{11}O_{39}\{SnC_6H_4-C\equiv C-C_6H_4NH_2\}] K_{Sn}[ArNH_2]$

**Figure S1.**  $^1H$  NMR (300 MHz) and  $^{31}P$  (121 MHz, framed inset) spectra of  $K_{Sn}[ArNH_2]$  in  $CD_3CN$ .

**Figure S2.** Comparison of experimental (lower trace) and calculated (upper trace) isotopic peaks for the ions  $[PW_{11}O_{39}\{SnC_6H_4-C\equiv C-C_6H_4NH_2\}]^{4-}$ ,  $[PW_{11}O_{39}\{SnC_6H_4-C\equiv C-C_6H_4NH_2\}.H]^{3-}$ ,  $[PW_{11}O_{39}\{SnC_6H_4-C\equiv C-C_6H_4NH_2\}.TBA]^{3-}$  and  $[PW_{11}O_{39}\{SnC_6H_4-C\equiv C-C_6H_4NH_2\}.2TBA]^{2-}$  of  $K_{Sn}[ArNH_2]$

##### Synthesis and characterizations of $(TBA)_3[PW_{11}O_{39}\{(SiC_6H_4-C\equiv C-C_6H_4NH_2)_2O\}] K_{Si}[ArNH_2]$

**Figure S3.**  $^1H$  NMR (300 MHz) and  $^{31}P$  (121 MHz, framed inset) spectra  $K_{Si}[ArNH_2]$  in  $CD_3CN$ .

**Figure S4.** Comparison of experimental (upper trace) and calculated (lower trace) isotopic peaks for the ions  $[PW_{11}O_{39}\{(SiC_6H_4-C\equiv C-C_6H_4NH_2)_2O\}]^{3-}$  and  $[PW_{11}O_{39}\{(SiC_6H_4-C\equiv C-C_6H_4NH_2)_2O\}.TBA]^{2-}$  of  $K_{Si}[ArNH_2]$

##### Synthesis and characterizations of $(TBA)_6[P_2W_{17}O_{61}\{(SiC_6H_4-C\equiv C-C_6H_4NH_2)_2O\}] D_{Si}[ArNH_2]$

**Figure S5.**  $^1H$  NMR (300 MHz) and  $^{31}P$  (121 MHz, framed inset) spectra of  $D_{Si}[ArNH_2]$  in  $CD_3CN$ .

**Figure S6.** Comparison of experimental (upper trace) and calculated (lower trace) isotopic peaks for the ions  $[P_2W_{17}O_{61}\{(SiC_6H_4-C\equiv C-C_6H_4NH_2)_2O\}.H]^{5-}$ ,  $[P_2W_{17}O_{61}\{(SiC_6H_4-C\equiv C-C_6H_4NH_2)_2O\}.TBA]^{5-}$ ,  $[P_2W_{17}O_{61}\{(SiC_6H_4-C\equiv C-C_6H_4NH_2)_2O\}.2TBA]^{4-}$ ,  $[P_2W_{17}O_{61}\{(SiC_6H_4-C\equiv C-C_6H_4NH_2)_2O\}.3H]^{3-}$  and  $[P_2W_{17}O_{61}\{(SiC_6H_4-C\equiv C-C_6H_4NH_2)_2O\}.3TBA]^{3-}$  of  $D_{Si}[ArNH_2]$

#### Electrochemical Characterization

**Figure S7.** Cyclic voltammogram of 1 mM  $D_{Si}[ArNH_2]$  in  $CH_3CN$  (0.1 M TBAPF<sub>6</sub>) at a ITO electrode, potentials given versus SCE electrode, scan rate 0.3 V.s<sup>-1</sup>

**Figure S8.** Cyclic voltammogram of immobilized  $K_{Si}[Ar]$  in  $CH_3CN$  (0.1 M TBAPF<sub>6</sub>) at a ITO electrode, potentials given versus SCE electrode, scan rate 0.5 V.s<sup>-1</sup>. First cathodic peak  $E_{pc}$  at -0.369 V/SCE and the corresponding anodic peak  $E_{pa}$  at -0.350 V/SCE ( $E_{pa}-E_{pc}=0.019$  V;  $E_{1/2}=1/2(E_{pa}+E_{pc})=-0.360$  V)

**Figure S9.** Cyclic voltammogram of immobilized  $K_{Sn}[Ar]$  in  $CH_3CN$  (0.1 M TBAPF<sub>6</sub>) at a ITO electrode, potentials given versus SCE electrode, scan rate 0.5 V.s<sup>-1</sup>. First cathodic peak  $E_{pc}$  at -1.022V/SCE and the corresponding anodic peak  $E_{pa}$  at -0.987 V/SCE ( $E_{pa}-E_{pc}=0.035$ V,  $E_{1/2}=1/2(E_{pa}+E_{pc})=-1.004$  V)

**Table S1.** Variation of the apparent surface coverage  $\Gamma$  with the initial concentration of  $D_{Si}[ArNH_2]$  in solution and upon multiple electrograftings

#### Surface characterization

**Figure S10.** AFM image and profile of raw ITO as supplied roughness  $R_a = 3.244$  nm (average thickness  $M_a = 22.95$  nm should be 150 nm?)

**Figure S11.** C-AFM images of a double grafted  $D_{Si}[Ar]$  film onto ITO, left :topography, right: current map at -0.5V

**Figure S12.** FESEM image of a double grafted **Dsi[Ar]** film onto ITO, using a narrow potential range [0; -0.5 V] for the electrodeposition ( $\Gamma_2 = 1.36 \text{ } 10^{-10} \text{ mol.cm}^{-2}$ )

**Figure S13.** FESEM image of a **Dsi[Ar]** film electrodeposited onto ITO from **DSi[ArNH<sub>2</sub>]** using LiBF<sub>4</sub> as the supporting electrolyte (from cyclic-voltammetry :  $\Gamma_{2,\text{Li}} = 3.92 \text{ } 10^{-10} \text{ mol.cm}^{-2}$  if recorded in a LiBF<sub>4</sub> electrolyte and  $\Gamma_{2,\text{TBA}} = 1.02 \text{ } 10^{-10} \text{ mol.cm}^{-2}$  if recorded in a TBAPF<sub>6</sub> electrolyte)

**Figure S14.** FESEM images of **K<sub>Sn</sub>[Ar]** films electrodeposited onto ITO from **KSn[ArNH<sub>2</sub>]** /tBuONO (left, mono-grafting  $\Gamma_1 = 4.06 \text{ } 10^{-11} \text{ mol.cm}^{-2}$ ) or preisolated **K<sub>Sn</sub>[ArN<sub>2</sub><sup>+</sup>]** (right)

**Figure S15.** XPS survey of three **Dsi[ArN]** films electrodeposited onto ITO from **DSi[ArNH<sub>2</sub>]**. The three substrates have an increasing  $\Gamma$  values ( $\Gamma_2 = 1.35 \times 10^{-10} \text{ mol.cm}^{-2}$ ,  $\Gamma_4 = 3.51 \times 10^{-10} \text{ mol.cm}^{-2}$  and  $\Gamma_6 = 6.20 \times 10^{-10} \text{ mol.cm}^{-2}$  for double-, quadruple- and sextuple-grafting respectively), from top to bottom

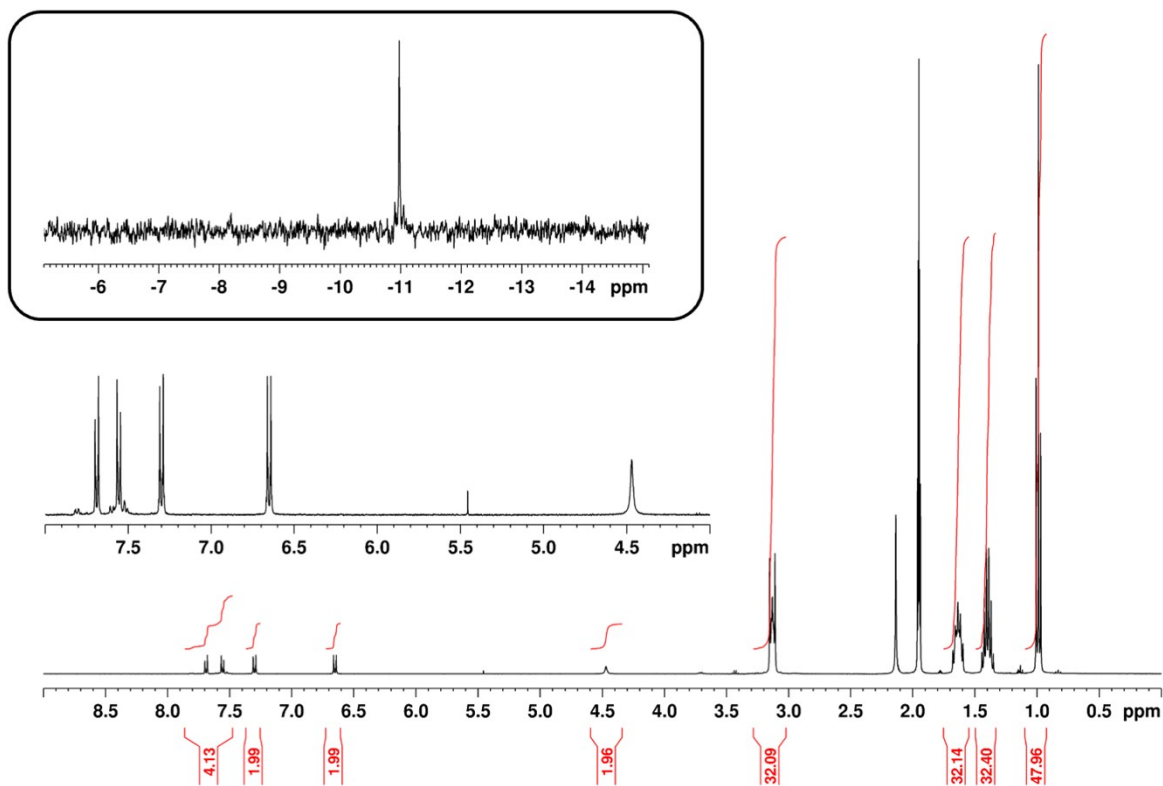
#### Memory tests

**Figure S16.** Representative examples of I-V characteristics of a **D<sub>Si</sub>[Ar]** film electrodeposited onto ITO: 95 % of WORM-type behavior (left) and 5% of Flash-type behavior (right) (double grafting)

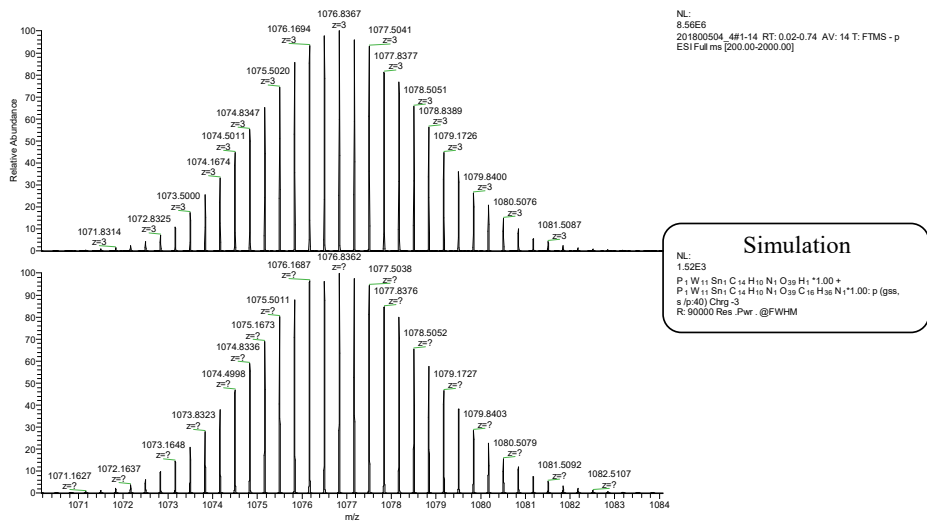
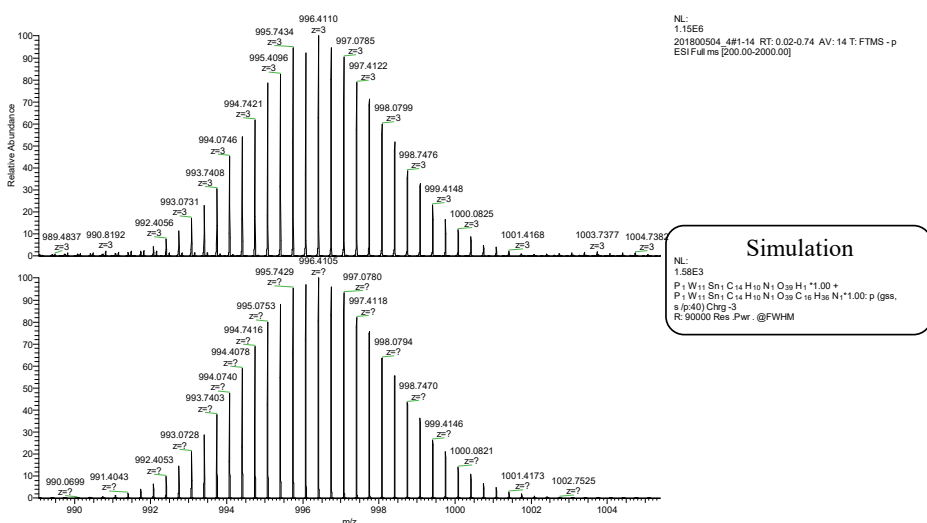
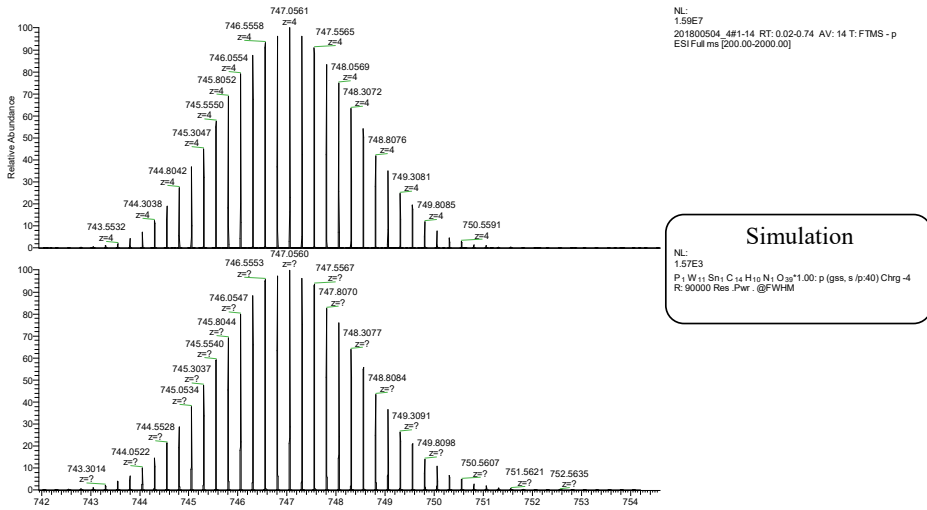
**Figure S17.** SET voltage variation for a given substrate (in orange or in green) and from a substrate to another

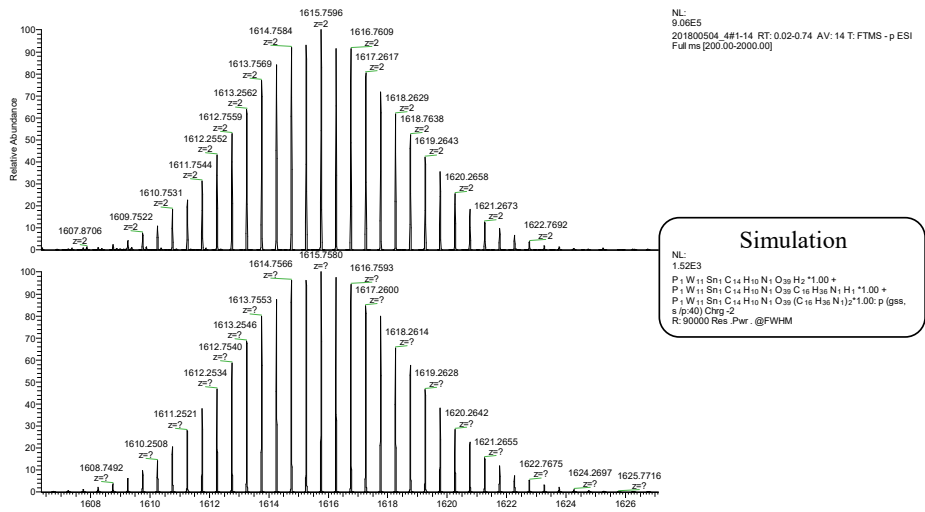
**Figure S18.** Current stability over time at a 0.5V reading voltage

**Synthesis and characterizations of  $(\text{TBA})_4[\text{PW}_{11}\text{O}_{39}\{\text{SnC}_6\text{H}_4-\text{C}\equiv\text{C-C}_6\text{H}_4\text{NH}_2\}] \text{K}_{\text{Sn}}[\text{ArNH}_2]$**



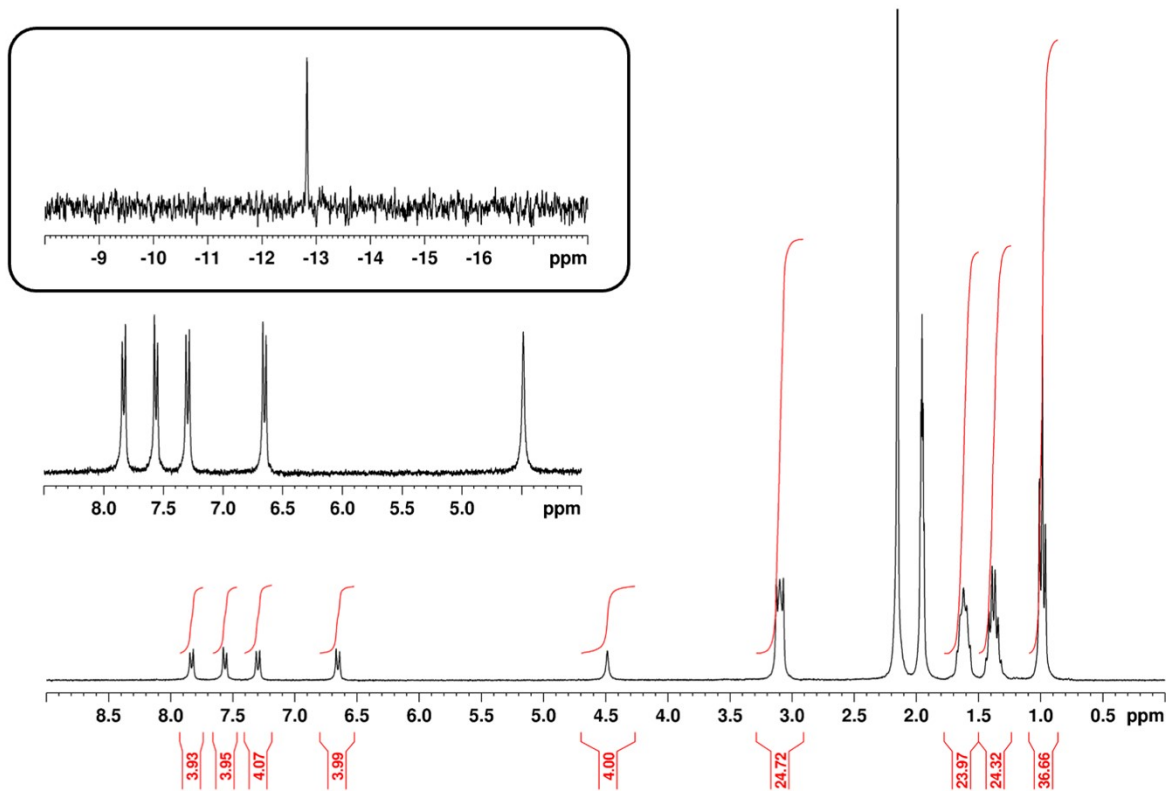
**Figure S1.**  $^1\text{H}$  NMR (400 MHz) and  $^{31}\text{P}$  (162.0 MHz, framed inset) spectra of  $\text{K}_{\text{Sn}}[\text{ArNH}_2]$  in  $\text{CD}_3\text{CN}$ .



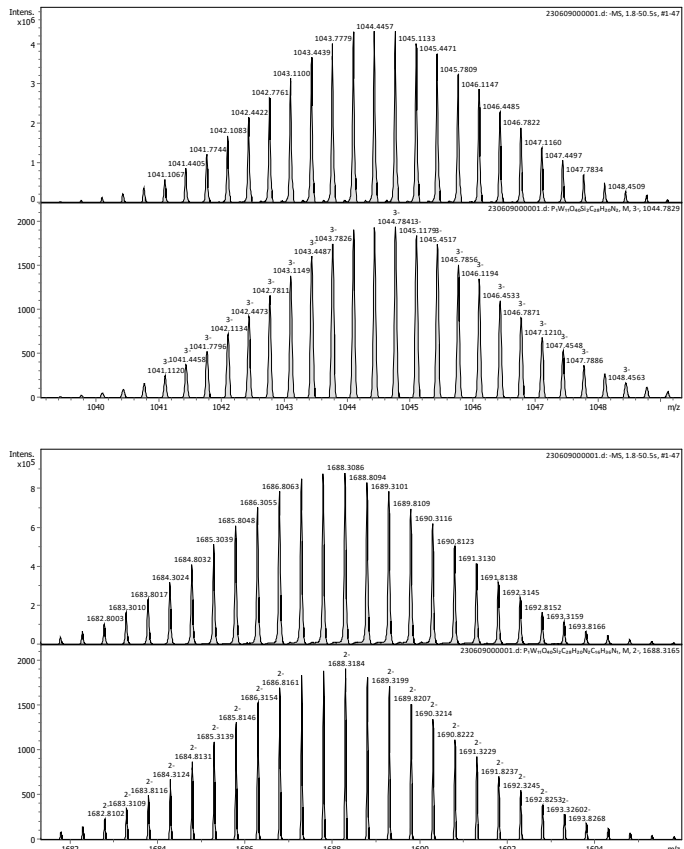


**Figure S2.** Comparison of experimental (lower trace) and calculated (upper trace) isotopic peaks for the ions  $[PW_{11}O_{39}\{SnC_6H_4-C\equiv C-C_6H_4NH_2\}]^{4-}$ ,  $[PW_{11}O_{39}\{SnC_6H_4-C\equiv C-C_6H_4NH_2\}.H]^{3-}$ ,  $[PW_{11}O_{39}\{SnC_6H_4-C\equiv C-C_6H_4NH_2\}.TBA]^{3-}$  and  $[PW_{11}O_{39}\{SnC_6H_4-C\equiv C-C_6H_4NH_2\}.2TBA]^{2-}$  of  $K_{Sn}[\text{ArNH}_2]$

**Synthesis and characterizations of  $(\text{TBA})_3[\text{PW}_{11}\text{O}_{39}\{\text{SiC}_6\text{H}_4-\text{C}\equiv\text{C}-\text{C}_6\text{H}_4\text{NH}_2\}_2\text{O}\}] \text{K}_{\text{Si}}[\text{ArNH}_2]$**

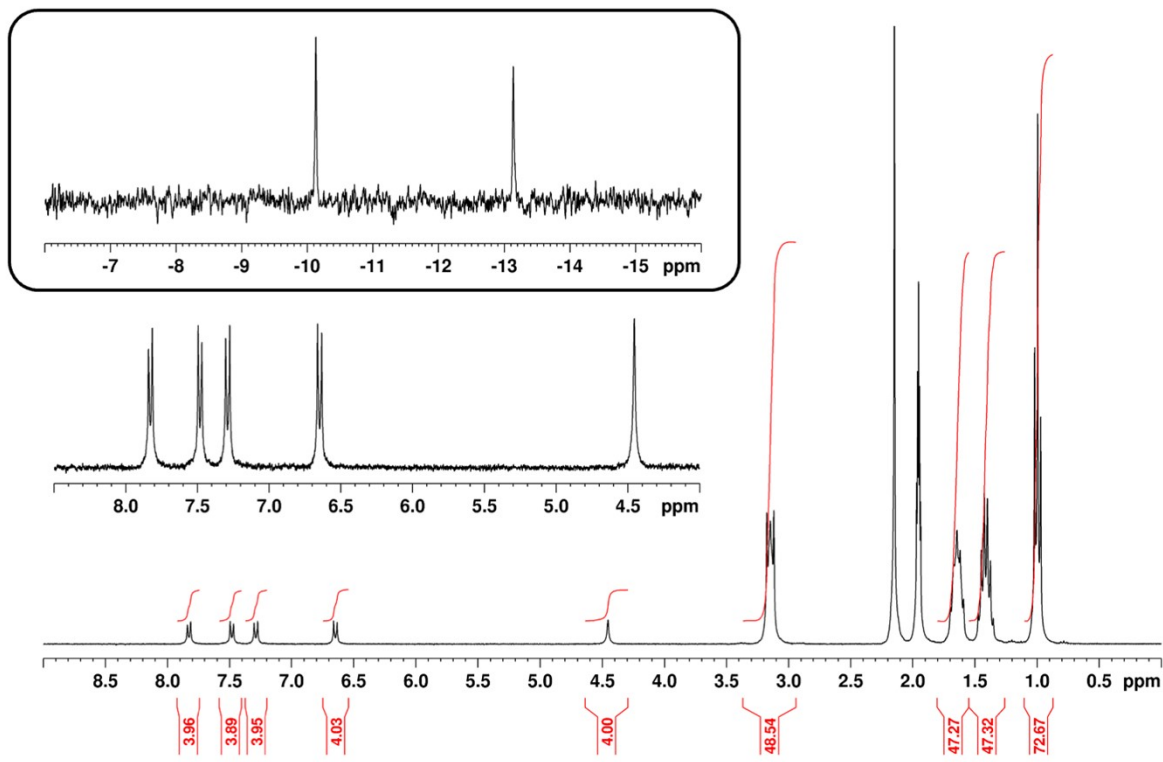


**Figure S3.**  $^1\text{H}$  NMR (300 MHz) and  $^{31}\text{P}$  (121.5 MHz, framed inset) spectra  $\text{K}_{\text{Si}}[\text{ArNH}_2]$  in  $\text{CD}_3\text{CN}$ .

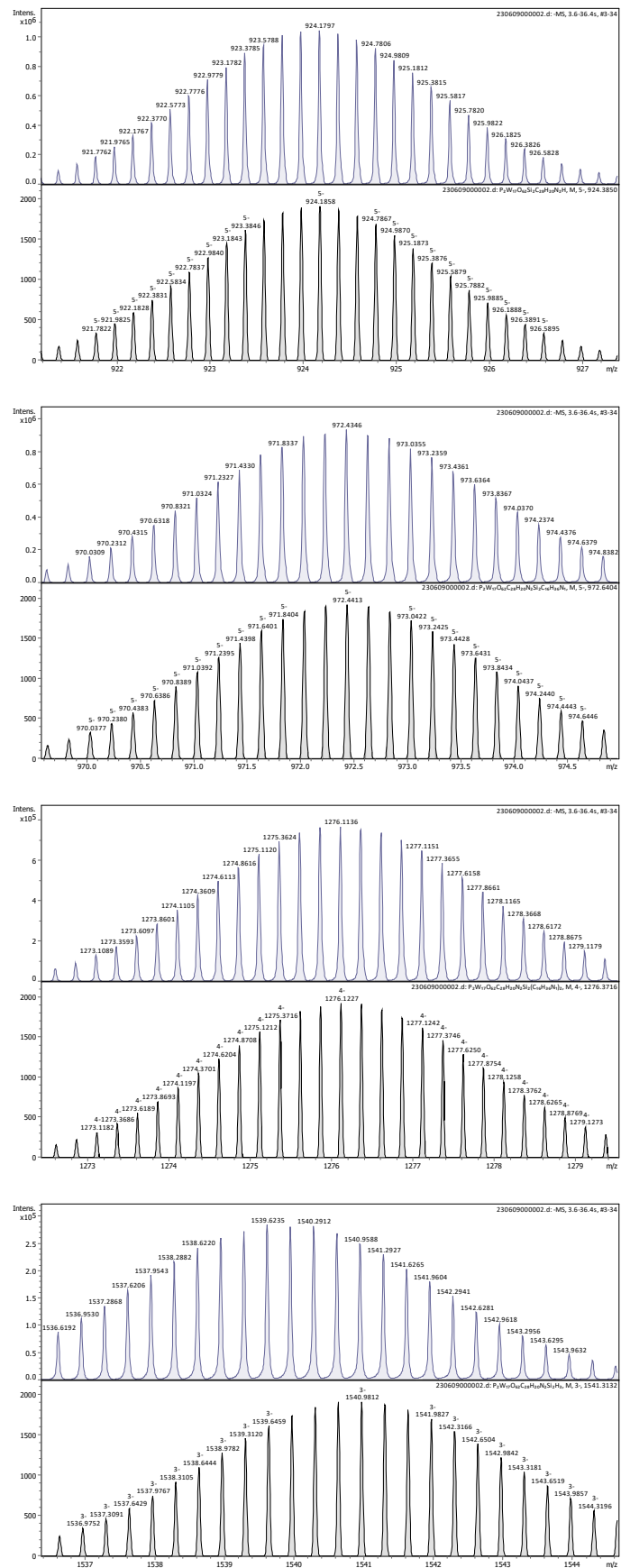


**Figure S4.** Comparison of experimental (upper trace) and calculated (lower trace) isotopic peaks for the ions  $[PW_{11}O_{39}\{(\text{SiC}_6\text{H}_4-\text{C}\equiv\text{C}-\text{C}_6\text{H}_4\text{NH}_2)_2\text{O}\}]^{3-}$  and  $[PW_{11}O_{39}\{(\text{SiC}_6\text{H}_4-\text{C}\equiv\text{C}-\text{C}_6\text{H}_4\text{NH}_2)_2\text{O}\} \cdot \text{TBA}]^{2-}$  of  $\text{K}_{\text{Si}}[\text{ArNH}_2]$

## Synthesis and characterizations of $(TBA)_6[P_2W_{17}O_{61}\{(\text{SiC}_6\text{H}_4-\text{C}\equiv\text{C}-\text{C}_6\text{H}_4\text{NH}_2)_2\text{O}\}] D_{\text{Si}}[\text{ArNH}_2]$



**Figure S5.**  $^1\text{H}$  NMR (300MHz) and  $^{31}\text{P}$  (121.5 MHz, framed inset) spectra of  $\mathbf{D}_{\text{Si}}[\text{ArNH}_2]$  in  $\text{CD}_3\text{CN}$



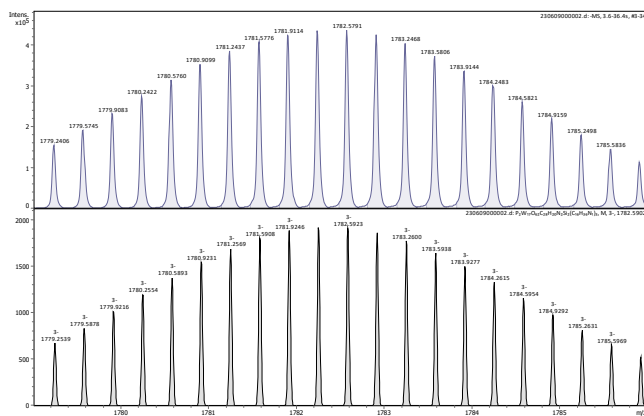


**Figure S6.** Comparison of experimental (upper trace) and calculated (lower trace) isotopic peaks for the ions  $[P_2W_{17}O_{61}\{(SiC_6H_4-C\equiv C-C_6H_4NH_2)_2O\}.H]^{5-}$ ,  $[P_2W_{17}O_{61}\{(SiC_6H_4-C\equiv C-C_6H_4NH_2)_2O\}.TBA]^{5-}$ ,  $[P_2W_{17}O_{61}\{(SiC_6H_4-C\equiv C-C_6H_4NH_2)_2O\}.2TBA]^{4-}$ ,  $[P_2W_{17}O_{61}\{(SiC_6H_4-C\equiv C-C_6H_4NH_2)_2O\}.3H]^{3-}$  and  $[P_2W_{17}O_{61}\{(SiC_6H_4-C\equiv C-C_6H_4NH_2)_2O\}.3TBA]^{3-}$  of  $D_{Si}[ArNH_2]$ .

## Electrochemical characterization

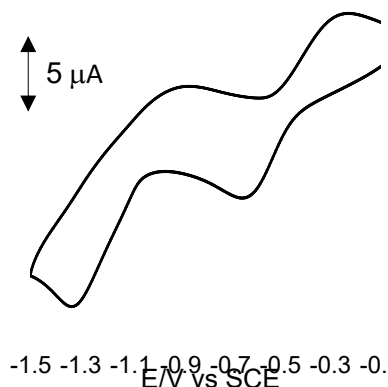


**Figure S7.** Cyclic voltammogram of 1 mM  $\mathbf{D}_{\text{Si}}[\text{ArNH}_2]$  in  $\text{CH}_3\text{CN}$  (0.1 M TBAPF<sub>6</sub>) at a ITO electrode, potentials given versus SCE electrode, scan rate 0.3 V.s<sup>-1</sup>

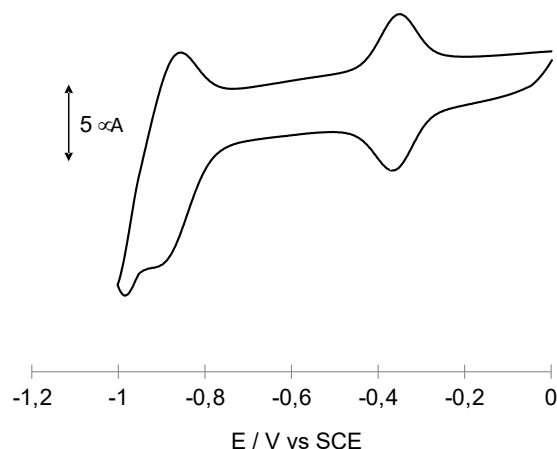


**Figure S8.** Cyclic voltammogram of immobilized  $\mathbf{K}_{\text{Si}}[\text{Ar}]$  in  $\text{CH}_3\text{CN}$  (0.1 M TBAPF<sub>6</sub>) at a ITO electrode, potentials given versus SCE electrode, scan rate 0.5 V.s<sup>-1</sup>. First cathodic peak  $E_{\text{pc}}$  at -0.369 V/SCE and the corresponding anodic peak  $E_{\text{pa}}$  at -0.350 V/SCE ( $E_{\text{pa}}-E_{\text{pc}}=0.019$  V;  $E_{1/2}=1/2(E_{\text{pa}}+E_{\text{pc}})=-0.360$  V)

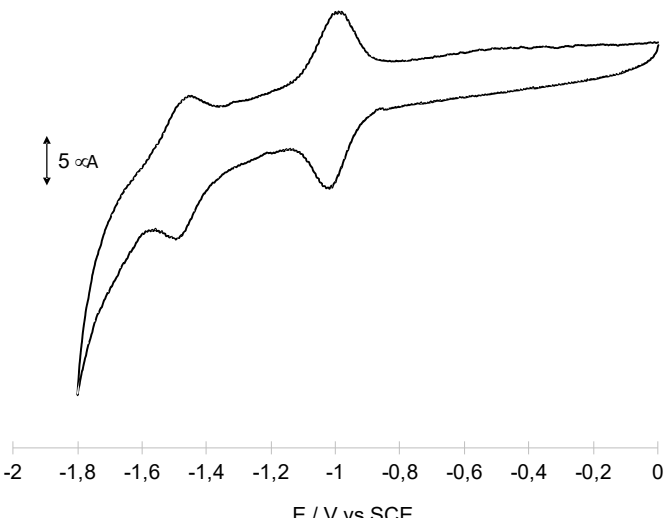


**Figure S9.** Cyclic voltammogram of immobilized  $\text{K}_{\text{Sn}}[\text{Ar}]$  in  $\text{CH}_3\text{CN}$  (0.1 M TBAPF<sub>6</sub>) at a ITO electrode, potentials given versus SCE electrode, scan rate 0.5 V.s<sup>-1</sup>. First cathodic peak  $E_{\text{pc}}$  at -1.022V/SCE and the corresponding anodic peak  $E_{\text{pa}}$  at -0.987 V/SCE ( $E_{\text{pa}}-E_{\text{pc}} = 0.035\text{V}$ ,  $E_{1/2} = 1/2(E_{\text{pa}}+E_{\text{pc}}) = -1.004\text{ V}$ )

Concentration (mM)	Concentration effect				Multi-graftings		
	<b>1</b>	0.2	0.5	2	1	1	1
$\Gamma_1 \times 10^{10} \text{ mol.cm}^{-2}$	<b>1.4</b>	0.2	0.9	1.2	0.9	1.1	1.3
$\Gamma_2$					<b>1.4</b>	1.4	1.7
$\Gamma_3$						2.2	3.7
$\Gamma_4$						<b>3.5</b>	6.2
$\Gamma_5$							2.9
$\Gamma_6$							<b>6.2</b>

**Table S1.** Variation of the apparent surface coverage  $\Gamma$  with the initial concentration of  $\text{D}_{\text{Si}}[\text{ArNH}_2]$  in solution and upon multiple electrograftings

### Surface characterization

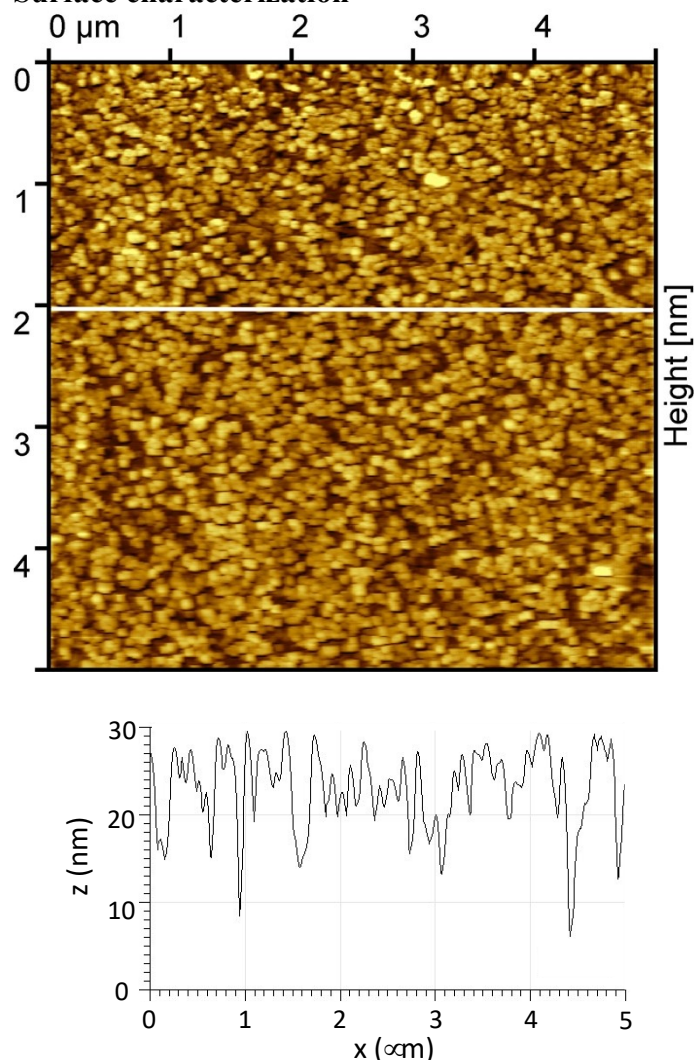


**Figure S10.** AFM image and profile of raw ITO as supplied roughness  $R_a = 3.244 \text{ nm}$  (average thickness  $M_a = 22.95 \text{ nm}$ )

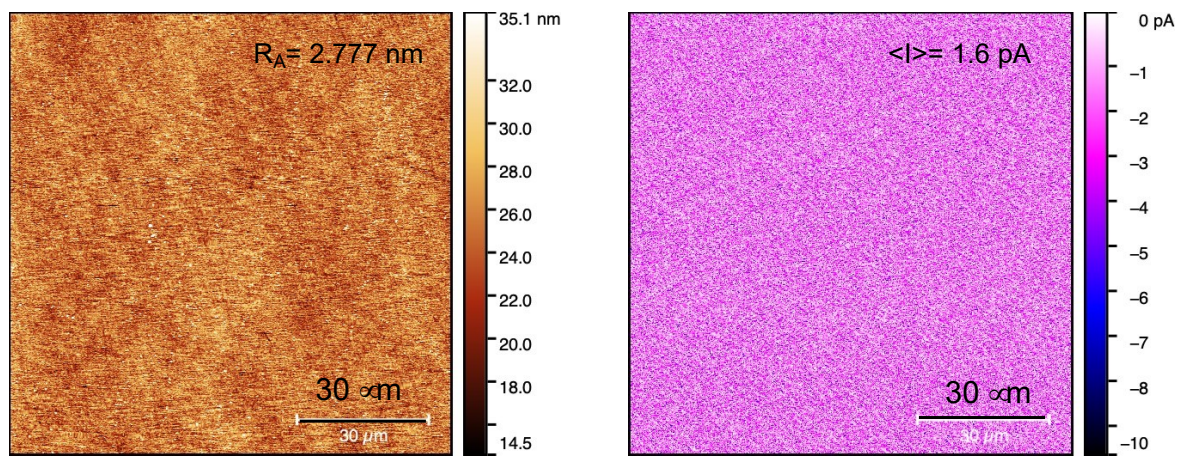


**Figure S11.** C-AFM images of a double grafted **Dsi[Ar]** film onto ITO, left :topography, right: current map at  $V_{\text{bias}} = -0.5\text{V}$

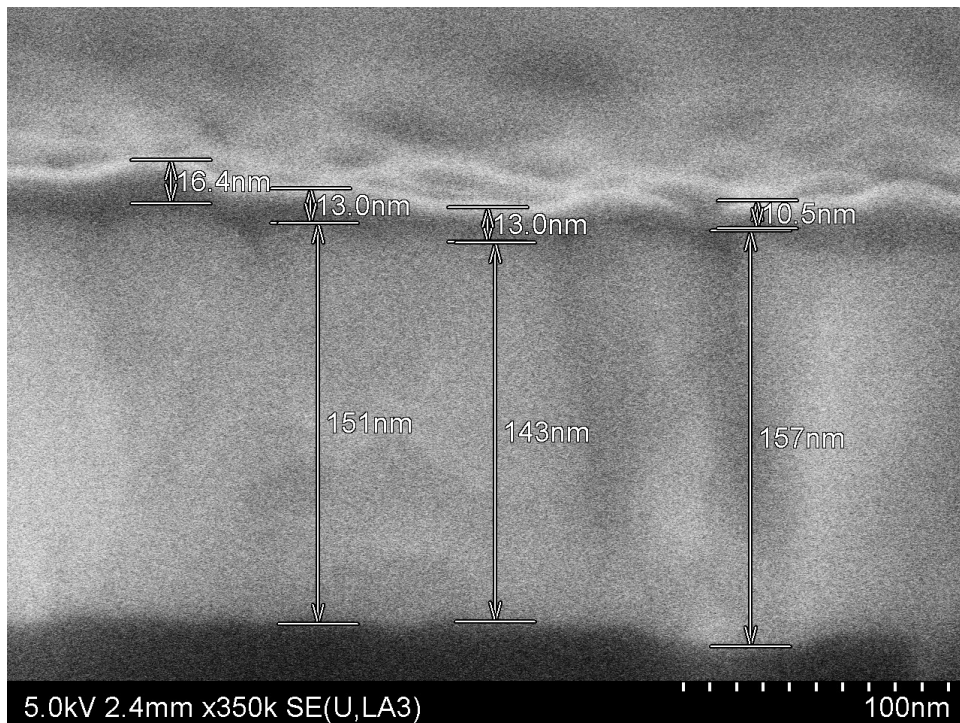


**Figure S12.** FESEM image of a double grafted **Dsi[Ar]** film onto ITO, using a narrow potential range [0; -0.5 V] for the electrodeposition

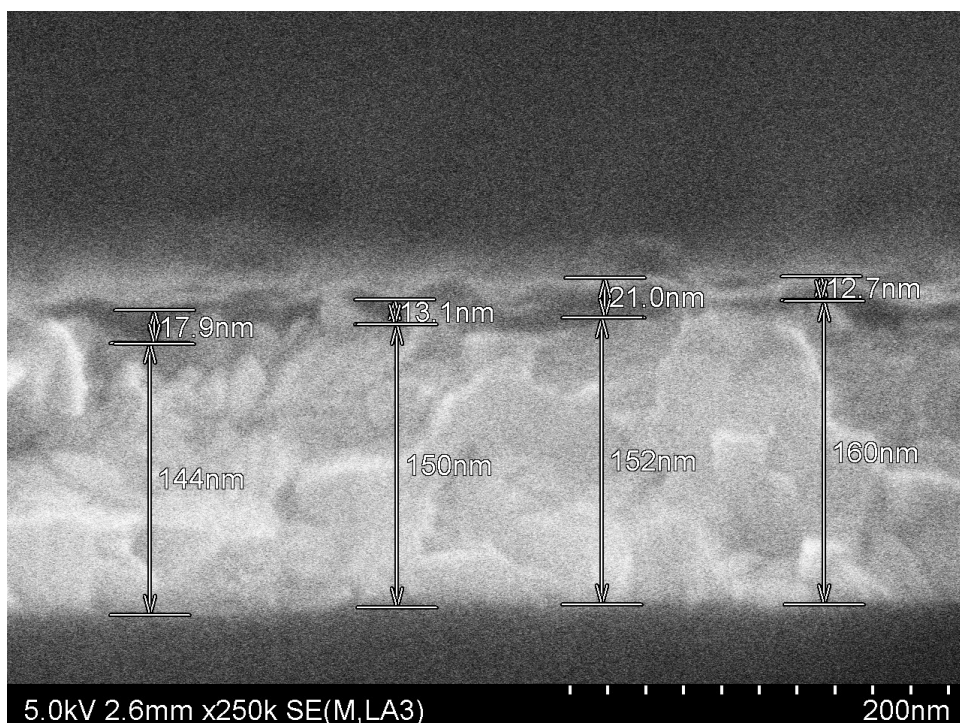


**Figure S13.** FESEM image of a **Dsi[Ar]** film electrodeposited onto ITO from **DSi[ArNH<sub>2</sub>]** using LiBF<sub>4</sub> as the supporting electrolyte (from cyclic-voltammetry :  $\Gamma_{2,Li} = 3.9 \cdot 10^{-10}$  mol.cm<sup>-2</sup> if recorded in a LiBF<sub>4</sub> electrolyte and  $\Gamma_{2,TBA} = 1.0 \cdot 10^{-10}$  mol.cm<sup>-2</sup> if recorded in a TBAPF<sub>6</sub> electrolyte )

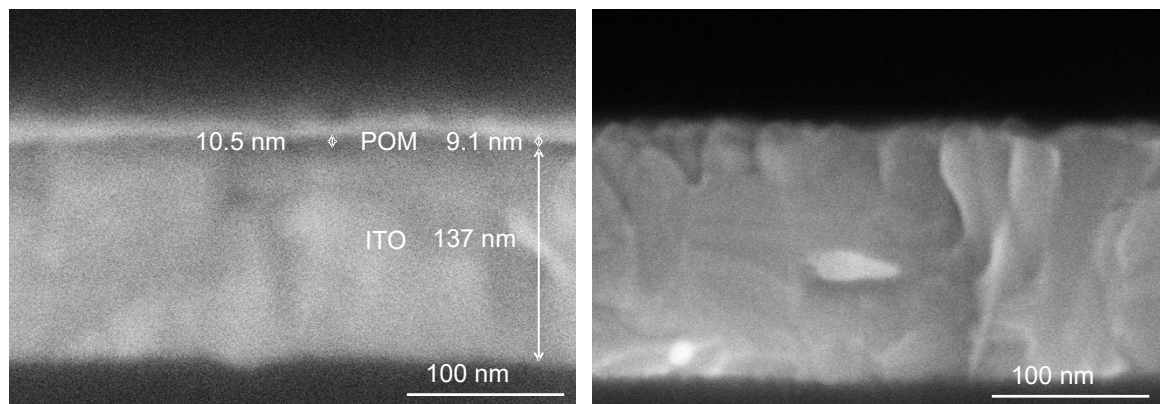


**Figure S14.** FESEM images of  $\text{K}_{\text{Sn}}[\text{Ar}]$  films electrodeposited onto ITO from  $\text{KSn}[\text{ArNH}_2]/\text{tBuONO}$  (left, mono-grafting) or preisolated  $\text{K}_{\text{Sn}}[\text{ArN}_2^+]$  (right)

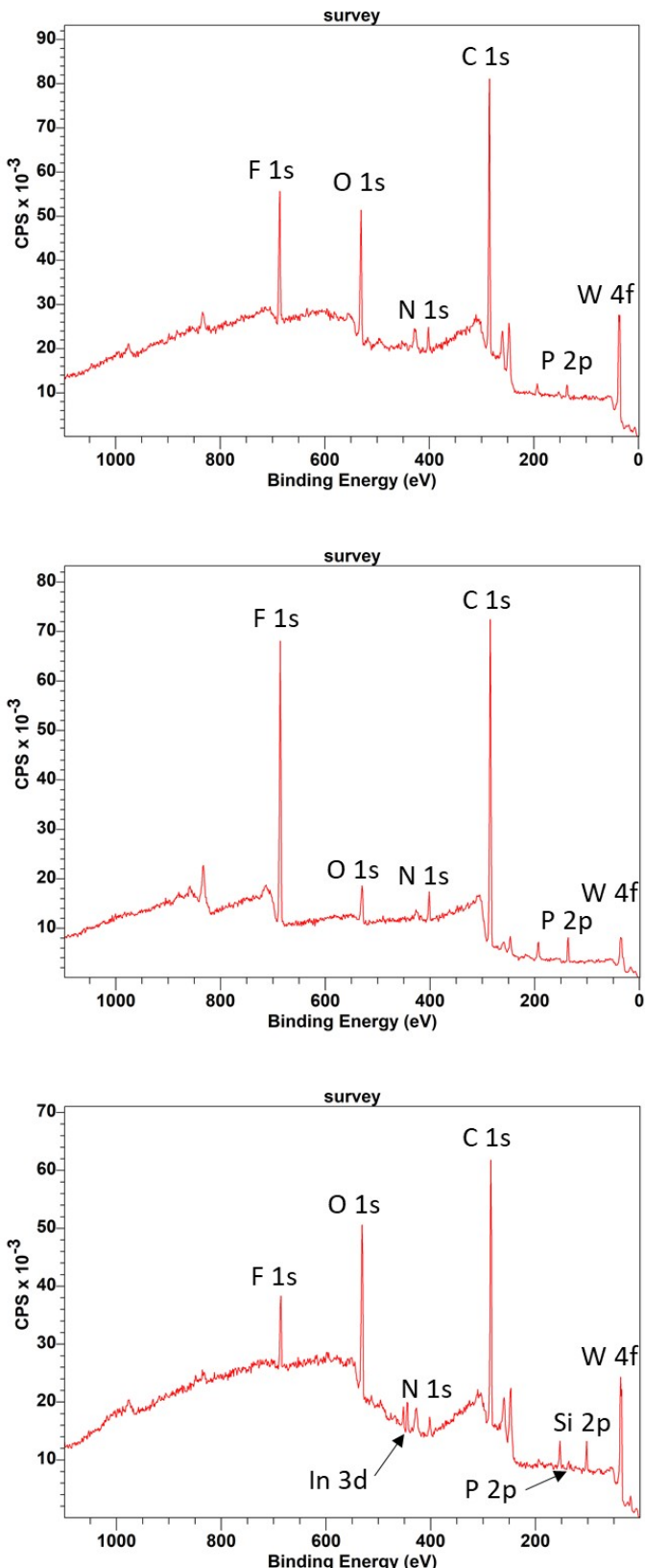


**Figure S15.** XPS survey of three **Dsi[ArN]** films electrodeposited onto ITO from **DSi[ArNH<sub>2</sub>]**. The three substrates have an increasing  $\Gamma$  values ( $\Gamma_2 = 1.35 \times 10^{-10} \text{ mol.cm}^{-2}$ ,  $\Gamma_4 = 3.51 \times 10^{-10} \text{ mol.cm}^{-2}$  and  $\Gamma_6 = 6.20 \times 10^{-10} \text{ mol.cm}^{-2}$  for double-, quadruple- and sextuple-grafting respectively), from top to bottom

An estimation of the thickness of the POM-based films could have been derived from the attenuation of the In photopeak from ITO. Three substrates of increasing  $\Gamma$  values for double-, quadruple- and sextuple-grafting respectively), prepared on the same day were studied. The In photopeak is hardly detectable on the survey spectra of two of them but is present on the third one (sextuple-grafting) The same substrates later on imaged by FESEM (see Figure 5 middle and bottom and Figure S15) displayed some thickness variability from place to place, yet with higher values than those that would allow to detect the In by XPS, which is technically limited to the analysis of a few nanometer thick materials (we roughly estimated a limit of 7-8 nm for a POM-based film using the QUASES program<sup>1,2</sup>). The XPS analyses indirectly confirm that our POM-films have an overall thickness of several nm but point out, in agreement with the SEM images, that the coverage is not uniform, thus allowing erratic In detection.

- (1) QUASES-IMFP-TPP2M Ver. 3.0 Inelastic Electron Mean Free Paths Calculated from the TPP-2M Formula, Code Written by Sven Tougaard. Copyright (c) 2000-2016 Quases-Tougaard Inc.
- (2) Shinotsuka, H.; Tanuma, S.; Powell, C. J.; Penn, D. R. Calculations of Electron Inelastic Mean Free Paths. X. Data for 41 Elemental Solids over the 50 eV to 200 KeV Range with the Relativistic Full Penn Algorithm: Calculations of Electron Inelastic Mean Free Paths. X. *Surf. Interface Anal.* **2015**, *47* (9), 871–888. <https://doi.org/10.1002/sia.5789>.

## Memory tests

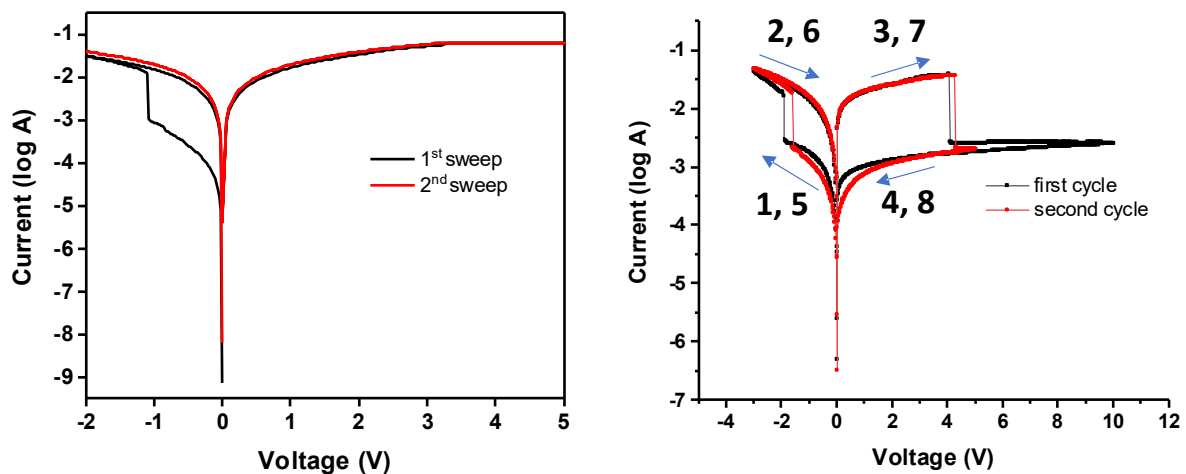


**Figure S16.** Representative examples of I-V characteristics of a  $\mathbf{D}_{\text{Si}}[\text{Ar}]$  film electrodeposited onto ITO: 95 % of WORM-type behavior (left) and 5% of Flash-type behavior (right) (double grafting)

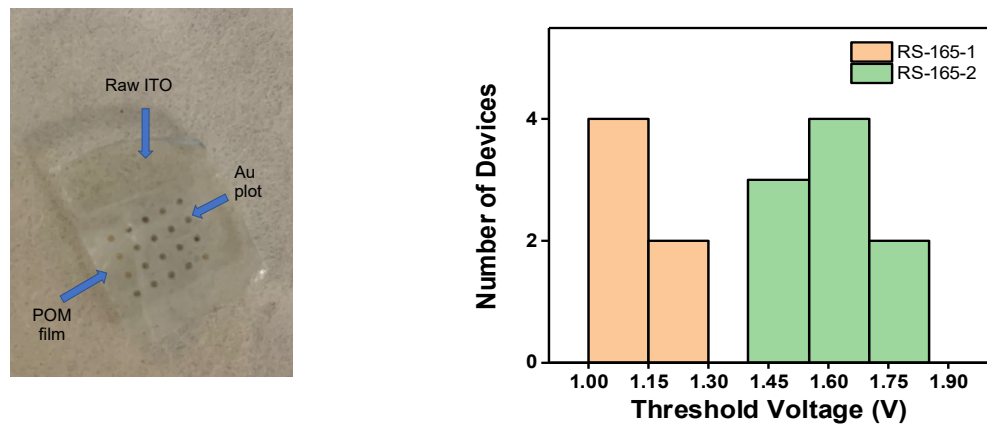


**Figure S17.** SET voltage variation for a given substrate (in orange or in green) and from a substrate to another

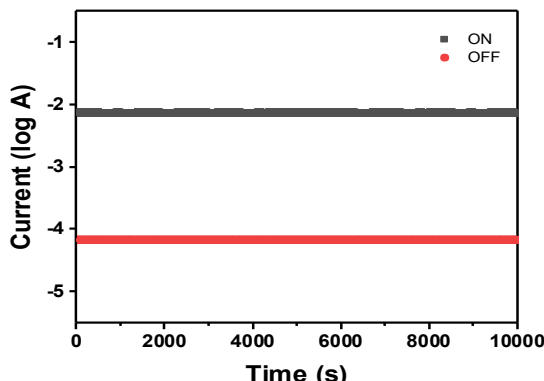


**Figure S18.** Current stability over time at a 0.5V reading voltage